Kinematic analysis of nanocomposite optical absorption of Ag/Ag_2O prepared by a green method

Esmaeil Shahriari (esmaeil.Phy@gmail.com)
Technical and Vocational University(TVU)
Morteza Raeisi
Shahrkord University

Research Article

Keywords: nanocomposite, Ag/Ag2O, UV absorption, Rietveld method, XRD

Posted Date: July 12th, 2022

DOI: https://doi.org/10.21203/rs.3.rs-1768794/v1

Abstract

In this report, silver and silver oxide nanocomposites are synthesized using a green method at different concentrations of silver nitrate. In this method, coelomic yellow liquid extracted from earthworms has been used as a silver nitrate reduction. The crystal structure of the obtained nanoparticles was analyzed by X-ray diffraction pattern and Rietveld method. The results show that with increasing the concentration of silver nitrate, the size and strain of silver oxide nanoparticles remained unchanged, but the size of silver nanoparticles increased and strain decreased. SEM images show uniform particle distribution, high density, and spherical geometric shape. By measuring and fitting the UV spectra of the nanocomposites, the weight percentage and the absorption peak of each component were determined. Accordingly, with increasing the concentration of silver nitrate, the absorption peak for silver nanoparticles is shifted to the higher wavelengths and for silver oxide nanoparticles is almost constant. Also, the weight percentage of silver oxide remains almost constant, and increases for silver nanoparticles. In the framework of a simple kinematic model, it is shown that its origin can be related to the different reactions speed of conversion of silver nitrate to silver and silver oxide.

Introduction:

In the last two decades, nanotechnology has made great strides due to its applications in various fields such as industry, agriculture and medicine and has become one of the most extensive research fields. Nanoparticles exhibit unique and valuable physical and chemical properties. At this scale, particles show different and interesting physical properties such as electrical and thermal conductivity, magnetic, mechanical and optical, as well as different chemical and biological properties due to high surface to volume ratio, high reactivity [1–3].

Various physical and chemical methods for the synthesis of nanoparticles are now widely used. However, these methods are usually expensive, costly, and potentially hazardous to the environment. [4–6]. Hence, it is necessary to replace cost-effective methods that are environmentally immune and safety.

Mineral nanoparticles composed of metals and their metal oxides such as silver, zinc, gold, copper have a wide range of applications. For example, gold nanoparticles are used in the design of electrical circuits with high conductivity and silver in the sterilization of medical equipment and drug preparation [7]. Among all synthesized metal nanoparticles, silver nanoparticles are the most widely used and show their superiority in various consumer products, more than 25 cases [8]. These nanoparticles are mostly used as antibacterial, antifungal and antiviral agents.

Over the past decade, it has been proven that many biological systems, including plants [9], bacteria [10], yeasts [11], fungi [12], and metabolites in these organisms can be reduced by proteins to convert mineral metal ions into metal nanoparticles.

Due to the potential of proteins in the coelomic yellow liquid produced by earthworms to regenerate the metal elements needed by the soil, metal oxides such as calcium, magnesium and potassium are predicted, which have the ability to convert metal ions to nanoparticles. Therefore, it is expected to be able to prepare silver

nanoparticles and its oxide from the precursor material, silver nitrate, by the process in vitro to extract liquid from the earthworm body [13, 14].

In the present work, a species of earthworm Eisenia foetida has been used to extract nanoparticles in the form of silver composite and its oxide. The extraction and purification process of coelomic liquid and production of nanoparticles were carried out in a simple route. Then the structural characteristics and optical properties of the sample are measured and analyzed. An interesting feature of this method is that complex compounds or impurities such as ammonia that are associated with coleomic fluid have not been observed in the chemical composition of the nanoparticles. The Ag and Ag2O phases in the nanocomposite have been well formed based on the measured their optical properties. By analyzing the results of X-ray template and absorption spectra separately, an excellent consistency in determining the weight percentage and size of nanoparticles of silver and oxide phases has been observed.

Material And Methods:

The samples were prepared by the following procedures in which brief experimental diagram was shown in Fig1:

Preparation of ceolomic fluid:

50 to 60 adult worms with grown genital warts are removed from the soil and washed with water. Then locate the worms in a container of cold water for 2 hours to drain their intestinal contents and then rinse. Next, add 15 cc of deionized water to the container including the worms, and by using a 9-volt book battery, electric shocks are applied to the worms for 10 seconds with 20 repetitions. This action causes the extraction of yellow coelomic fluid from the worms. After separating liquid, the worms are returned to the environment. The extracted coelomic from the worms' body was placed within a refrigerated centrifuge at 4 ° C for 15 minutes at 13,000 rpm to produce a clear yellow liquid.

Preparation of nanocomposite:

5 ml of coelomic with a certain amount of silver nitrate is dissolved twice in 50 ml of deionized water to give a pale solution. The container including the solution is covered with aluminum foil and placed in a dark room for three days. After this time, the solution turns brown, which indicates the production of silver nanoparticles. The solution is centrifuged again at 4 ° C for 20 minutes at 15,000 rpm. Silver nanoparticles precipitate at the bottom of the Falcon tube and a colorless liquid is placed on top of the tube. The previous step is repeated for 4 times by adding deionized water and methanol to wash the nanoparticles. Finally, the precipitate of the obtained nanocomposite is exposed to the open air to dry.

Instrumentations:

X-ray diffraction (XRD) patterns of the samples were obtained using a diffractometer (Bruker, Billerica, MA, USA) with CuKα radiation of 0.15407 nm wavelength at 40 kV acceleratingvoltage and 40 mA electric current. The samples were scanned over a 10–80◦ range of diffraction angle (2θ). Rietveld refinement of the XRD data

(using a High Score Plus software) was used to determine the phase composition, crystallite size and unit cell parameters of nanocomposites.

UV-Vis spectra were collected using the UV-Vis spectrophotometer (Shimadzo UV3100) working in the range 200–800 nm.

Scanning electron microscopy (SEM) analyses of the samples were performed using a microscopeVEGA\\TESCAN-LMU. For SEM analyses, the powdered samples were ultrasonically dispersed in ethanol for a few minutes.

Results And Discussion:

XRD:

Fig.2 shows XRD pattern of synthesized Ag/Ag2O composite nanopowder at different concentrations of silver nitrate. The peaks of all samples matched well with cubic structure for both pure Ag and Ag2O nanocrystalls. The diffraction peaks position for silver nanoparticles at 2teta are 38.1, 44.3, 64.5 and 77.5, which are corresponding the planes of (111), (200), (220) and (311), respectively. The remained two others peaks at angles 26.7, 54.9 is related to silver oxide that are indicated with planes of (111), (022) for Ag2ONPS component. The XRD spectra obtained were confirmed with the standard spectra of JCPDS no. 00-004-0783 and 01-076-1489 for Ag and Ag2O, respectively.

To determine the percentages, sizes and strains of appeared phases in composite, an analysis of measured XRD patterns were accomplished for various concentrations. The obtained results was listed in Table1.

Table1: The size and strain of prepared nanocomposite for each peaks of samples.

2tet	S1		S2		S3		S4		S5	
	St.	Size	St.	Size	St.	Size	St.	Size	St.	Size
26.7	1.17	14.3	1.16	14.3	0.84	19.80	0.69	24.2	0.67	24.9
38.1	0.87	13.5	0.57	20.6	0.30	39.1	0.14	84.1	0.18	64.6
44.3	0.74	13.7	0.36	27.9	0.25	40.6	0.29	35.5	0.14	72.1
54.9	0.62	13.5	0.63	13.3	0.54	15.5	0.69	12	0.69	11.9
64.5	0.49	14.8	0.51	14	0.45	15.9	0.46	15.8	0.41	17.4
77.5	0.24	25.8	0.23	26.3	0.22	26.9	0.26	23.6	0.17	36.9

Table2: The weight percentage and mean size and strain of Ag and Ag2O nanoparticle at different concentration.

Sample	C(mM)	Ag%	Ag size	Ag Strain	C(Ag)	Ag2O%	Ag2O Size	Ag2O Strain	C(Ag2O)
S1	10	70	17.7	0.58	5.38	30	14.1	0.90	2.3
S2	15	84	22.2	0.42	10.86	16	13.8	0.89	2.1
S3	20	87	30.6	0.31	15.4	13	17.6	0.70	2.3
S4	30	88	39.7	0.29	23.57	12	18.1	0.69	3.2
S5	45	90	47.7	0.23	36.81	10	18.4	0.68	4.1

The concentrations of silver nanoparticles and its oxide based on obtained the diffraction pattern data, are calculated and listed in Table 2. As can be seen, the concentration of silver oxide nanoparticles did not change significantly and are independent of the initial silver nitrate. The origin of this behavior can be related to the competition of two kinematic processes. The one is due to chemical conversion of oxide to silver by ammonia and also the rate of agglomeration of oxide to nanoparticles.

Here, a simple kinematic model was used to temporal behavior of components concentration in solution. In this model, the synthetic chemical processes include, silver nitrate to silver and silver oxide by coelomic liquid as a reduction. In addition, the reaction of silver oxide to silver by derivative ammonia of coleomic is considered as follows:

$$2\,AgNO_3 + \text{"}coelomic\text{"} \rightarrow 2\,Ag + 2\,NO_2 + O_2 \quad (1)$$

$$4\,AgNO_3 + \text{"}coelomic\text{"} \rightarrow 2\,Ag_2O + 4\,NO + 3\,O_2 \quad (2)$$

$$3\,Ag_2O + 2\,NH_3 \rightarrow 6\,Ag + N_2 + 3\,H_2O \quad (3)$$

If c1, c2 and c3 is considered the concentration values as a function of time for silver nitrate, silver and silver oxide, respectively, the rate of their changes is expressed by the following equations.

$$\frac{dc_1}{dt} = -2(k_1 + k_2)c_1 \quad (4)$$

$$\frac{dc_2}{dt} = 2k_1c_1 + 2k_3c_3 \quad (5)$$

$$\frac{dc_3}{dt} = k_2c_1 - k_3c_3 \quad (6)$$

Where k1, k2 and k3 are the rates of chemical reactions in processes 1, 2 and 3, respectively.

The analytical solution of the three coupled differential equations 1 to 3 will be as follows:

$$c_1(t) = c_0 e^{-2(k_1+k_2)t}$$

$$c_2(t) = \frac{2k_1c_0}{2(k_1+k_2)} c_0(1-e^{-2(k_1+k_2)t}) + \frac{4k_2k_3c_0}{2(k_1+k_2)-k_3}[(\frac{1}{k_3} - \frac{1}{2(k_1+k_2)}) + \frac{e^{-2(k_1+k_2)t}}{2(k_1+k_2)} - \frac{e^{-k_3t}}{k_3}]$$

$$c_3(t) = \frac{2k_2}{2(k_1+k_2)-k_3} c_0(e^{-k_3t} - e^{-2(k_1+k_2)t})$$

Where c_0 is the initial value of the silver nitrate concentration. As an example for the typical values of k_1=0.2, k_2=0.1, k_3=0.01, the general behavior of the concentration is shown in Figure 3 for an initial concentration of c_0 (10mM).

As expected, the concentration of silver nitrate in the preliminary times decreases rapidly. While the concentration of silver oxide, first increases and then decreases with a smooth trend by converting to silver atoms in the process (3). In contrast, the amount of silver increases in the early times with a faster rate and then in higher times with a slower rate. After a long time, the silver value reaches the initial silver nitrate concentration. In this model, the general behavior of concentrations are independent of the chemical reaction rates.

However, the final values of silver and silver oxide from Table 2 differ from this model. This may be due to the beginning of agglomeration process concurrent with the synthesis procedure. The process of nucleation and growth of nanoparticles are complex and strongly dependent on the interaction between them, it is not considered in this model. But by comparing the current model predictions with the results of Table 2, it can be inferred that the agglomeration of silver oxides prevents the complete conversion of silver oxide molecules to silver atoms. Therefore, the presence of this process causes the maximum concentration of silver oxides reaches from 1.2 mM to 2.3 mM (Fig.3).

On the other hand, in the analysis of diffraction pattern measurements, it has been shown that the size of silver oxide nanoparticles is almost constant and independent of the initial concentration of silver nitrate (Table 1). Although the rate of agglomeration of silver oxides depends on the mechanism of interaction, but for this case it seems that the growth stage of the smaller nanoparticles will continue up to larger nanoparticles no more than approximately 17 nm.

By investigating the width of diffraction peaks related to silver oxide nanoparticles at different concentrations, it can be pointed that no noticeable changes are observed. As well known the width of each diffraction peak is equal to the sum of the width contributions due to the particle size and the strain. Because the size of silver oxide nanoparticles has been almost constant, so their widths will also be constant. As a result, the share of width due to particle strain is expected to remain constant. Therefore, this leads to a constant strain value of silver oxide nanoparticles as shown in Table 2. However, in the case of strain in silver nanoparticles, by changing the overall width of the diffraction peaks and changing the size of the silver nanoparticles, it can be inferred that it has a slow downward trend.

SEM:

SEM micrographs of the samples along with the grain size distributions are shown in Figures 4a to 4e. As can be seen, the grains are uniform, high density and spherical form. Each grain is composed of silver and silver oxide nanoparticles. Therefore, the grain size depends on the weight percentage of nanoparticles in the samples. The average grain size is expected to be more than the average size of the nanocrystals. By extracting data from SEM images, the average grain size changes in the range of 23nm to 63nm. These values are also consistent with the results obtained from diffraction pattern data.

Absorption spectra:

The absorbance spectra of three substances, silver nitrate as precursor, coelomic as reducing agent and polyvinyl pyrrolidine as stabilizer are shown in Figure 5. As can be seen, there is no absorption peak in the visible area. In the reactions, silver nitrate is converted to silver and silver oxide nanoparticles, but the stabilizing substance remains unchanged in solution.

The measured absorption spectra of samples at different concentrations from 10mM to 45mM with subtracting PVP absorbing effect at room temperature show in Fig.5. There is no interaction between PVP and nanocomosites, also no presence reduction agent and precursor effect.

The same peak was observed for all nanocomposite samples at about 448 nm. As can be expected, the absorbance increases with increasing concentritation of the nanocomposites. Since the nanocomposite is composed of two components, silver and silver oxide, and assuming that the interaction between the two components is negligible, the total absorbance can be considered as a linear combination effect. Therefore, by fitting method and considering the Gaussian distribution, the contribution of both components can be determined.

Figure 6 shows the absorption behavior for a sample with a concentration of 10 mM by combining two Gaussian functions with different position peaks and widths. The peaks are located at 414nm and 471 for silver and silver oxide nanoparticles, respectively. Furthermore, the absorption contribution for silver nanoparticles is 77% and for its oxide nanoparticles is 23%. This result is consistent with the values obtained from XRD analysis. A brief of performed analysis for all of concentrations were presented in Table.1

Table3: The central peak, FWHM and weight percentage of each component of nanocomposite

Sample	Ag profiles				Ag2O profiles				Chi-square
	Peak (nm)	FWHM(nm)	A1	%	Peak(nm)	FWHM(nm)	A2	%	
S1	415+4	332+16	86+5	77	471+1	129+18	23+1	23	0.998
S2	420+4	268+6	101+4	86	472+1	114+9	16|+5	14	0.999
S3	423+2	319+6	171+6	89	469+1	124+2	21+2	11	0.999
S4	426+4	262+12	155+9	89.6	471+3	123+6	18+6	10.4	0.999
S5	432+4	258+10	230+12	90	471+2	105+9	26+9	10	0.999

As can be seen from Table 3, as the concentration of silver nitrate increases, the portion of silver nanoparticles increases. This behavior is consistent with X-ray diffraction pattern data. In addition, for silver particles, the nanoparticle absorption peak moves to higher wavelengths, while the silver oxide nanoparticle absorption peak remains almost constant. On the other hand, the same behavior has been observed with size for silver and silver oxide nanoparticles (Table 2). Due to the surface plasmons resonant effect of nanoparticles, it is expected for silver shifts to higher wavelengths and for silver oxide remains unchanged.

Conclusion:

Nanocomposites of Ag and Ag2O were prepared from silver nitrate at different concentration by a green reduction agent, coelomic liquid in which were extracted from earthworms. The XRD measurement and Rietveld analysis show that

the concentration of silver oxide nanoparticles did not change significantly and are independent of the initial silver nitrate. It is due to chemical conversion of oxide to silver by ammonia and also the rate of agglomeration of oxide to nanoparticles. Furthermore, the concentration of Ag nanoparticles proportionally changed with silver nitrate concentration. Also the results show that the estimated size and strain of silver oxide nanoparticles is almost constant and independent of the initial concentration of silver nitrate while for silver nanoparticles, the size increased and strain decreased. For silver oxide it seems that the growth stage of the smaller nanoparticles will continue up to larger nanoparticles no more than approximately 17 nm. The UV measurements indicated that the average absorption peaks are placed at 414nm for silver and 471nm for silver oxide nanoparticles. The absorption contribution for silver nanoparticles is 77% and for its oxide nanoparticles is 23%. This result is consistent with the values obtained from XRD analysis. SEM images displayed that the grains are uniform, high density and spherical form and their the average size changes in the range of 23nm to 63nm. The proposed green synthetic method provides an opportunity to overcome the problems associated with the instability of the nanocomposite particles prepared in the form of a nanofluid. The present study emphasizes a sustainable and environmentally friendly manner relative to other methods.

Declarations:

Consent for publication

The Author warrants that the work has not been published before in any form except as a preprint, that the work is not being concurrently submitted to and is not under consideration by another publisher.

Ethics approval and consent to participate

Not applicable

Funding

The authors declare that no funds, grants, or other support were received during the preparation of this manuscript.

Competing Interests

The authors have no relevant financial or non-financial interests to disclose.

Availability of data and materials

The datasets generated during the current study are available from the corresponding author on reasonable request.

Authors' contributions

All authors contributed to material preparation, data collection and analysis. All authors read and approved the final manuscript.

Acknowledgements

Not applicable

References:

1. Sahoo, M.; Vishwakarma, S.; Panigrahi, C.; Kumar, J. Nanotechnology: Current applications and future scope in food. *Food Front.* **2021**, *2*, 3–22.
2. Maurer-Jones, M.A.; Gunsolus, I.L.; Murphy, C.J.; Haynes, C.L. Toxicity of engineered nanoparticles in the environment. *Anal. Chem.* **2013**, *85*, 3036–3049.
3. Shahriari E, Maleki Z, Zamiri R,. Linear and non-linear optical properties of Ag doped ZnS thin film. *Opt Quant Electron*, **2017.** V. 49. № 151. P. 1–12.
4. Kannan Badri Narayanan, Natarajan Sakthivel, Biological synthesis of metal nanoparticles by microbes, Advances in Colloid and Interface Science, 2010. V. 156. № 1-2. P. 1–13.
5. Gan P.P., ng S.H., Huang Y., Li S.F., Green synthesis of gold nanoparticles using palm oil mill effluent (POME): a low-cost and eco-friendly viable approach, Bioresour. technol. 2012., V. 113, P. 132–135
6. V. V. Makarov, A. J. Love, O. V. Sinitsyna, S. S. Makarova, I. V. Yaminsky, M. E. Taliansky, N. O. Kalinina, “Green” Nanotechnologies: Synthesis of Metal Nanoparticles Using Plants, ACTA nature VOL. 6 № 1 (20) 2014

7. Vance, M.E.; Kuiken, T.; Vejerano, E.P.; McGinnis, S.P.; Hochella, M.F., Jr.; Rejeski, D.; Hull, M.S. Nanotechnology in the real world: Redeveloping the nanomaterial consumer products inventory. Beilstein J. Nanotechnol. 2015, 6, 1769–1780
8. Pritam Kumar Dikshit, Jatin Kumar, Amit K. Das, Soumi Sadhu, Sunita Sharma, Swati Singh, Piyush Kumar Gupta and Beom Soo Kim, Green Synthesis of Metallic Nanoparticles: Applications and Limitations, Catalysts 2021, 11(8) 1-35
9. Akbarzadeh, R.; Dehghani, H. Sodium-dodecyl-sulphate-assisted synthesis of Ni nanoparticles: Electrochemical properties. Bull. Mater. Sci. 2017, 40, 1361–1369
10. Hua, S.; De Matos, M.B.; Metselaar, J.M.; Storm, G. Current trends and challenges in the clinical translation of nanoparticulate anomedicines: Pathways for translational development and commercialization. Front. Pharmacol. 2018, 9, 790.
11. Sriramulu, M.; Shanmugam, S.; Ponnusamy, V.K. Agaricus bisporus mediated biosynthesis of copper nanoparticles and its biological effects: An in-vitro study. Colloid Interface Sci. Commun. 2020, 35, 100254.
12. Kuppusamy, P.; Yusoff, M.M.; Maniam, G.P.; Govindan, N. Biosynthesis of metallic nanoparticles using plant derivatives and their new avenues in pharmacological applications—An updated report. Saudi Pharm. J. 2016, 24, 473–484.
13. Naseem, T. and Durrani, T., The role of some important metal oxide nanoparticles for wastewater and antibacterial applications: A review, Environmental Chemistry and Ecotoxicology, volume 3, 2021, Pages 59-75
14. Y. Chang Y. , H.C. Zeng, Controlled synthesis and self-assembly of single-crystalline CuO Nanorods and Nanoribbons Cryst. Growth Des., 4 (2), 397-402(2004).

Figures

Figure 1

A brief diagram of synthesis composite

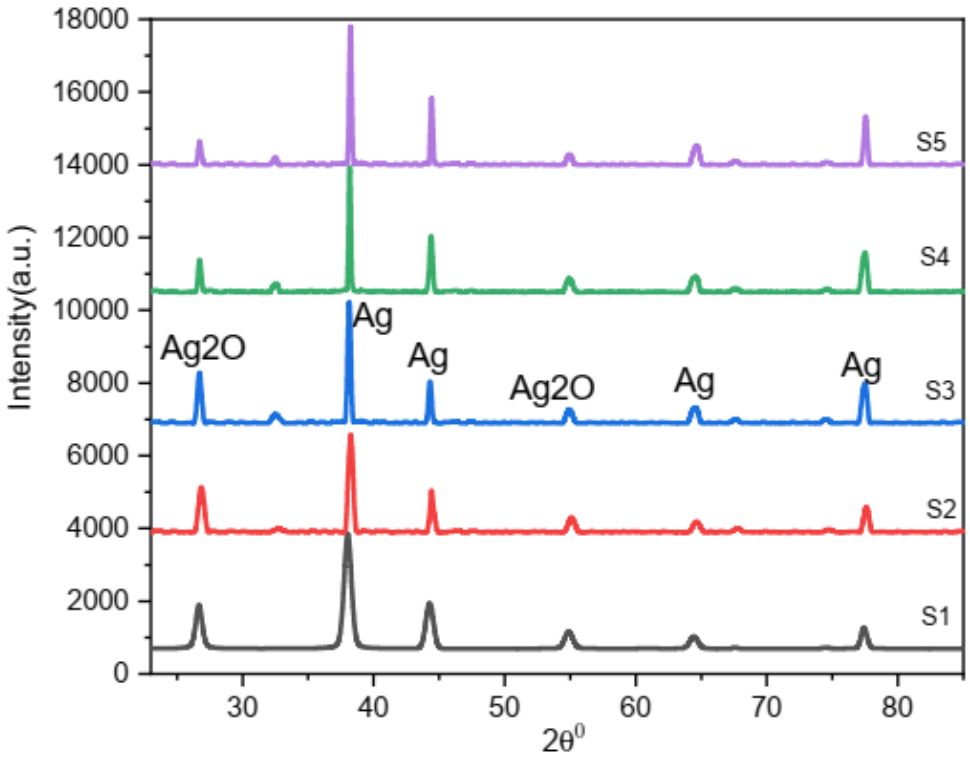

Figure 2

XRD pattern of nanocomposite at different concentration

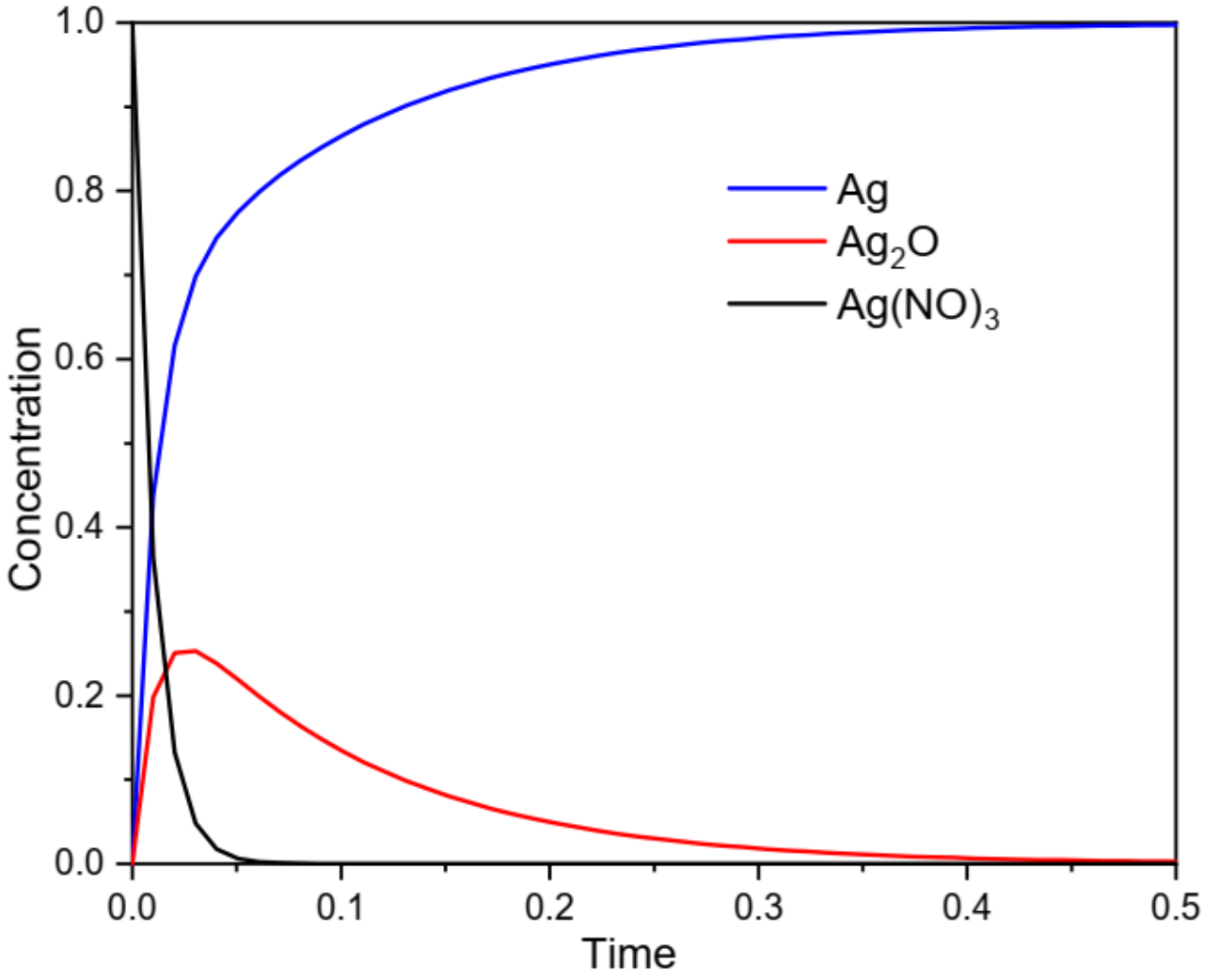

Figure 3

Time dependence of Ag and Ag2O nanoparticles formation.

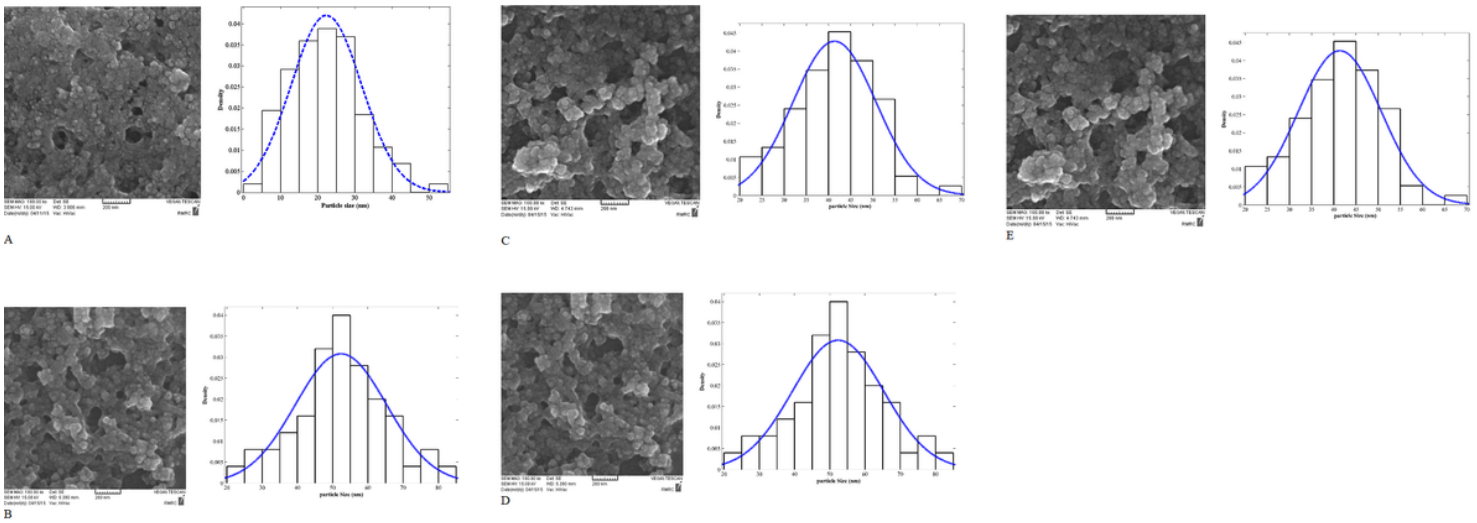

Figure 4

SEM'images and size distrbutions of nanocomposite at different concentration.

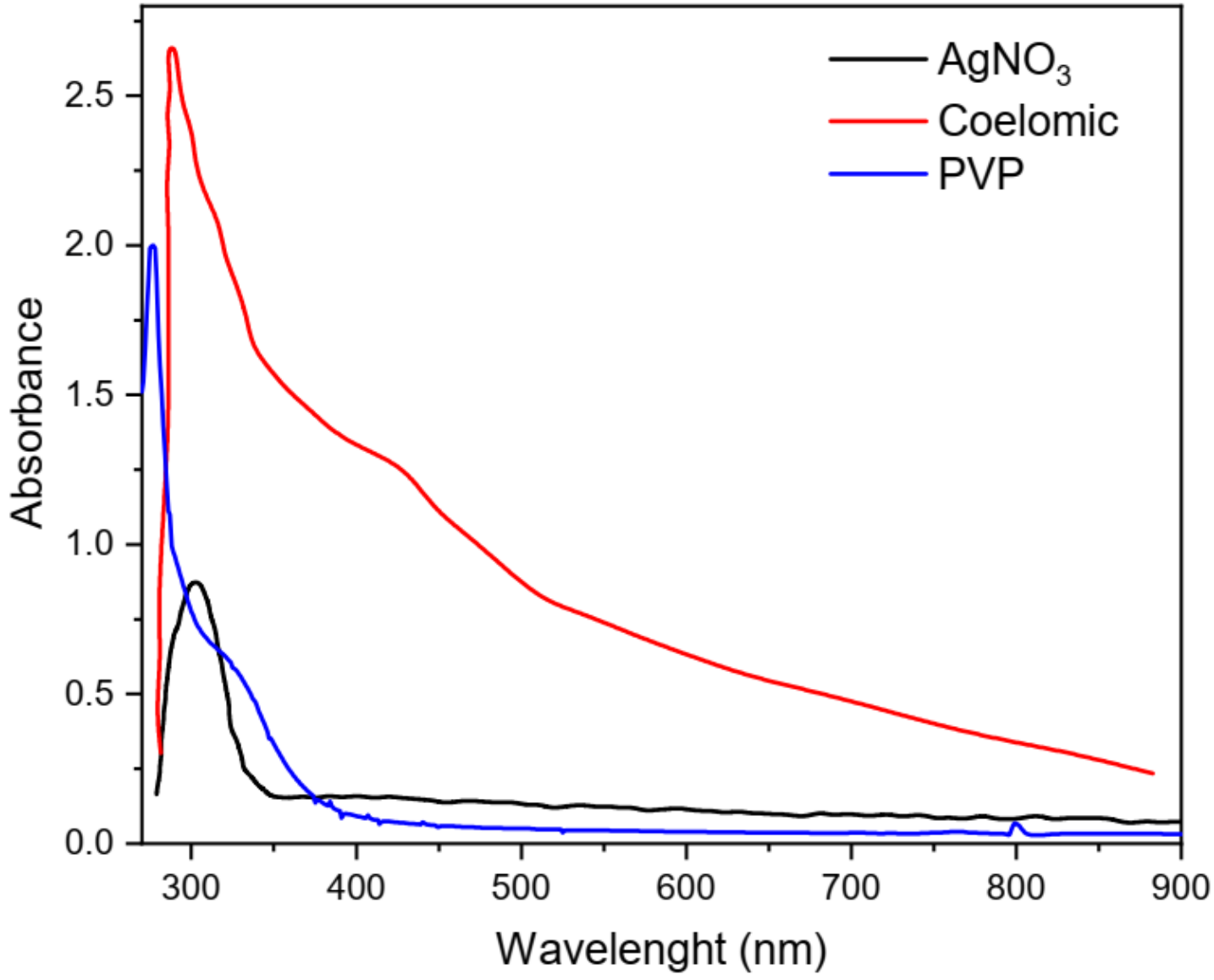

Figure 5

Absorption spectra of precursor material AgNO3, coelomic fluid and PVP.

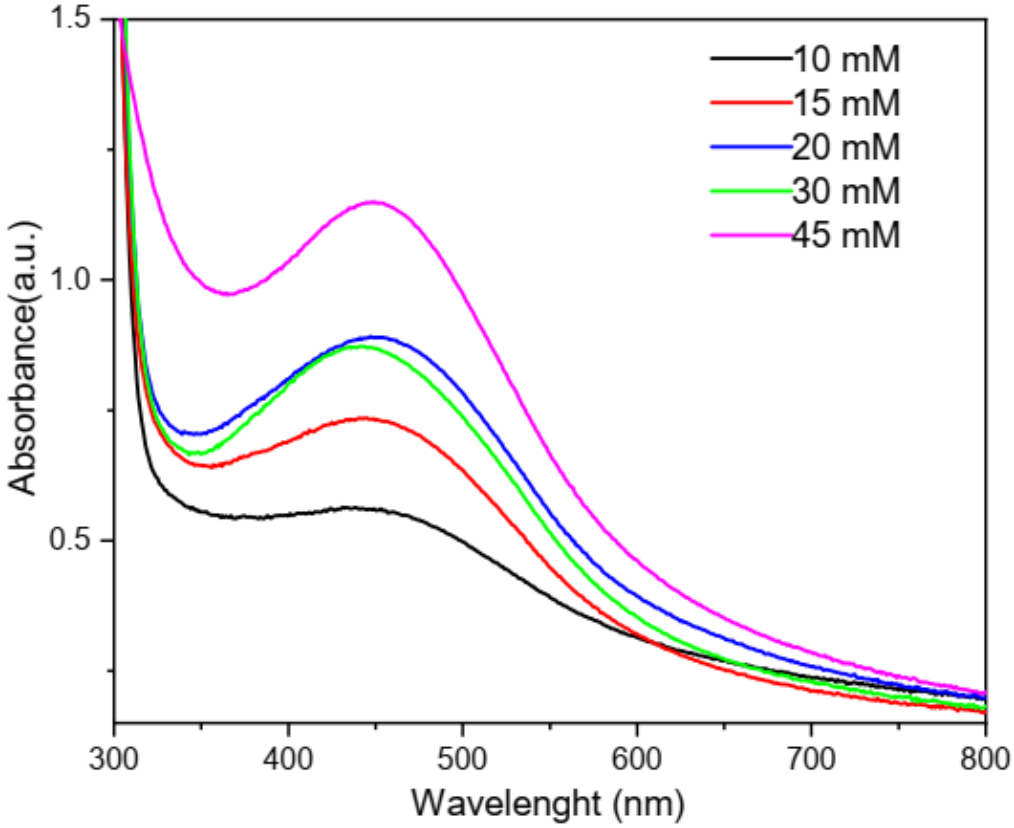

Figure 6

UV-visible absorption of nanocomposite at concentration 10 to 45 mM.

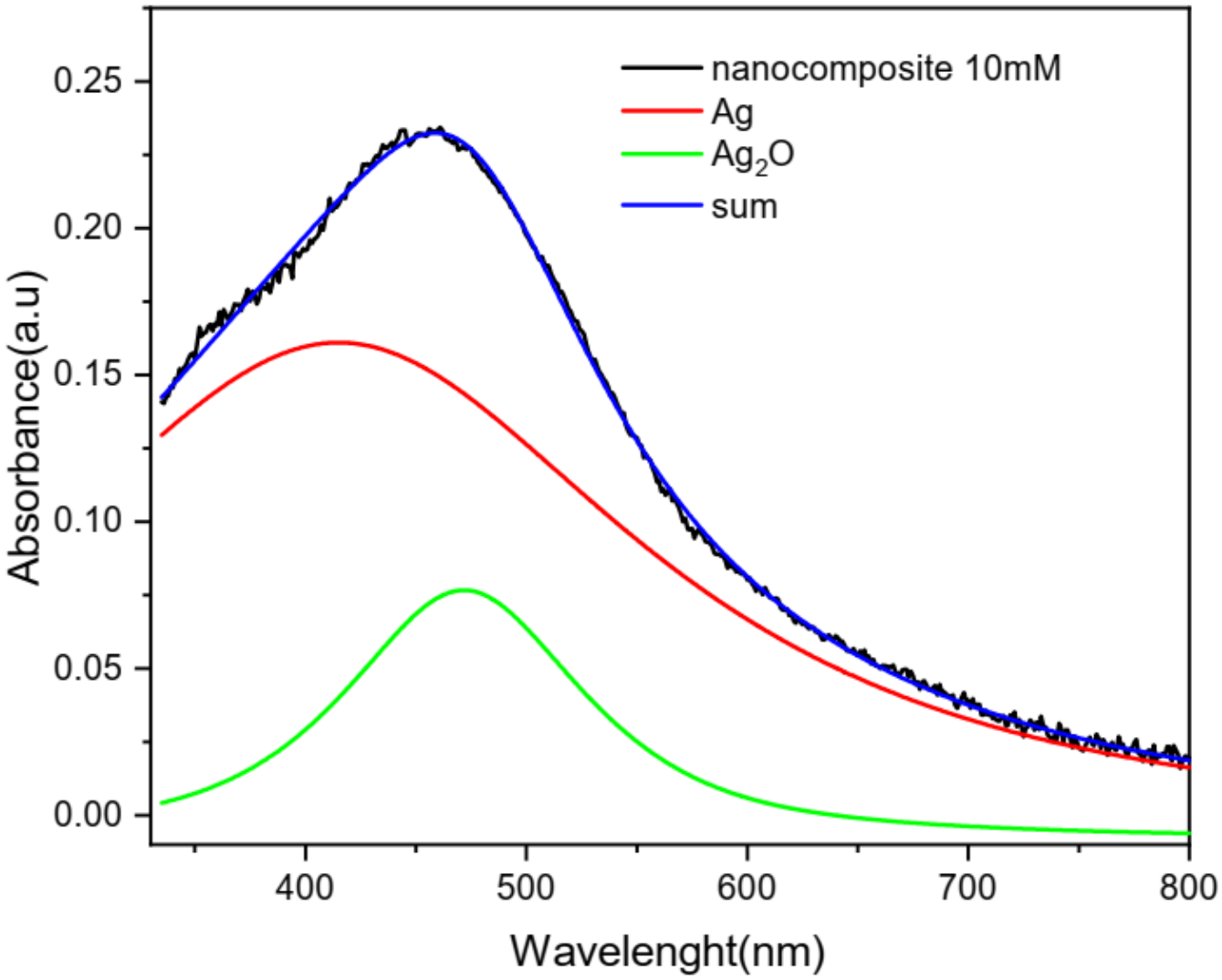

Figure 7

The Gaussian components of absorbtion spectra of Ag and Ag2O in nanocomposite for 10mM.